(23) Ramo, S.; Whinnery, J. R.; van Duzer, T. *Fields and Waves in Communication Electronics*; Wiley: New York, 1965.
(24) King, R. W. P.; Harrison, C. W. *Antennas and Waves: A Modern Approach*; MIT Press: Cambridge, 1969; Chapter 9.
(25) Slatkavitz, K. J.; Uden, P. C.; Barnes, R. M. *J. Chromatogr.* **1986**, *355*, 117-126.
(26) Sullivan, J. J. Detectors. In *Modern Practice of Gas Chromatography*, Grob, R. L., Ed.; Wiley: New York, 1977.
(27) Bradley, C.; Carnahan, J. W. *Anal. Chem.* **1988**, *60*, 858-863.

RECEIVED for review October 6, 1989. Accepted February 5, 1990.

Characterization of a Computerized Photodiode Array Spectrometer for Gas Chromatography–Atomic Emission Spectrometry

James J. Sullivan* and Bruce D. Quimby

Hewlett-Packard Company, Route 41 & Starr Road, Avondale, Pennsylvania 19311

An atomic emission detector (AED) for gas chromatography offers improved sensitivity and selectivity over earlier AEDs for all major elements found in gas chromatographic effluents. It is based on a novel water-cooled, microwave-powered plasma light source, which is described in a companion paper. A photodiode array (PDA) improves selectivity by several orders of magnitude by means of real-time multipoint background correction. A computer-controlled spectrometer, based on a concave holographic grating, has a flat focal plane along which the PDA can be moved. The wavelength range is from 160 to 800 nm. With the PDA, special algorithms provide automated wavelength calibration, autofocusing, and measurements of intensity, wavelength, and line width. Wavelength measurements are precise to 0.004 nm, and wavelength changes to positions far from calibration wavelengths are accurate to 0.008 nm. The detection of an elemental emission line and its spectral background makes use of many simultaneous signals from the PDA. These signals are combined into a pair of digital filters, called a recipe. The recipe structure provides optimal signal detection and has null response to, or is orthogonal to, the background spectrum. The signal and background portions of a chromatogram are recorded separately, so that the selectivity can be improved after the run is completed. The minimum detectable level is 20 pg/s for chlorine and 13 pg/s for bromine. An advanced type of recipe has null response to two different interfering spectra. This improves selectivities under routine conditions by a factor between 3 and 10. For chlorine and bromine, molar selectivites with respect to carbon of 24 000 and 13 000, respectively, have been achieved. Spectra are acquired continuously during a chromatogram. They are used to confirm the elemental identification of GC peaks and to make new recipes. An example is given where these spectra allow a subtle spectral change that degraded selectivity to be diagnosed and corrected. The effects of misalignment and of drift on performance are measured. Improvements in sensitivity and selectivity are reported for sulfur and for chlorine detection. Recipes are tested for sensitivity to wavelength errors and for sensitivity to shifts between multiple instruments. Over several days, responses are typically constant to 1%.

INTRODUCTION

As described by LaFreniere, Fassel, and Eckels (*1*), the ideal element-specific chromatographic detector would detect all elements in real time at parts-per-billion levels, determine empirical formulas, and measure multiple elements simultaneously. It would be simple and inexpensive, linear over 3 to 4 orders of magnitude, and compatible with chromatographic conditions. It would also have low dead volume. For gas chromatography, perhaps two additional characteristics should be stipulated. Selectivity with respect to other elements should be greater than 10 000, and totally automatic operation should be possible.

This paper describes a detector for gas chromatography based on atomic emission spectroscopy (GC-AES), which shows some progress toward the ideal case mentioned above. A previous paper described the new microwave-induced plasma used in the detector and its water-cooled discharge tube and efficient microwave system (*2*). This paper concentrates on the detector's sensitivity and selectivity achieved using a specialized spectrometer, a photodiode array (PDA), and optimized signal processing algorithms in a modified chromatography workstation.

In GC-AES of nonmetallic elements, the selectivity relative to carbon rarely exceeds a few hundred. Several approaches have been used to improve this. Even with very high resolution systems, such as echelle spectrometers and some interferometers, there can still be significant spectral interference in GC applications (*3-6*).

Background correction is necessary to achieve needed levels of selectivity in GC-AES. There are many methods of correcting for broad-band spectral interference using measurements at neighboring wavelengths. Some instruments use a cyclic shift in wavelength, so that background measurements are made alternatively with signal measurements. An oscillating refractor plate after the entrance slit is one way to do this (*7-9*).

Scanning instruments can collect data on either side of a line, during scanning, for background correction. There can be inaccuracies because the background and signal measurements are not obtained simultaneously (*10*).

Instruments with fixed optics, such as direct readers, sometimes use the detector outputs from other channels for background correction (*11*, *12*). In gas chromatographic applications, a version of this method is to subtract a calibrated amount of the signal on a carbon channel from the signal on a heteroatom channel (*13*).

A PDA can perform real-time multipoint background correction. It has a large number of pixels, or detecting elements, each of which is active 100% of the time (*14*). The large number of pixels gives flexibility in designing a background correction algorithm so that many constraints can be satisfied. The simultaneous, nonmultiplexed nature of the pixel signals promises more precise background correction.

0003-2700/90/0362-1034$02.50/0

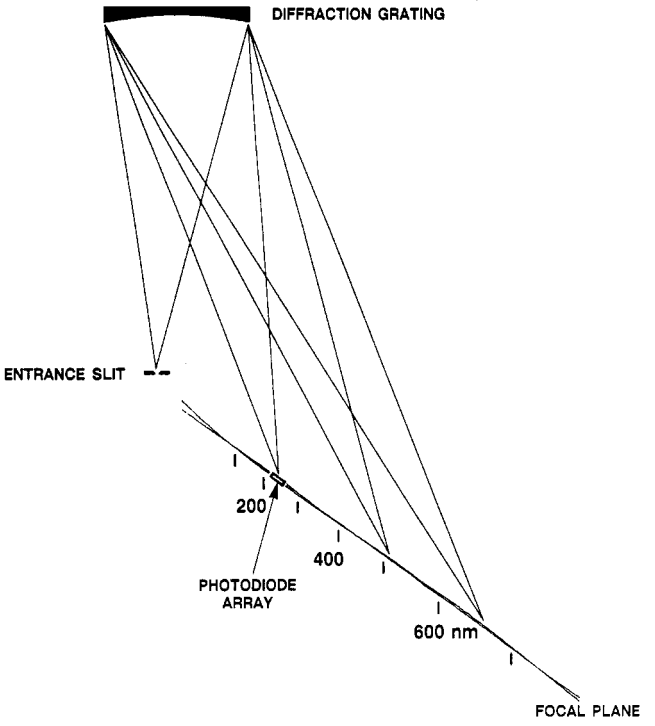

Figure 1. Schematic diagram of the spectrometer. Light from the entrance slit is diffracted and focused by the grating. The line of travel of the photodiode array is nearly coincident with the focal plane.

The PDA has become the detector of choice in low resolution spectrometers, such as those for UV–vis, and for detectors for liquid chromatography (*15*, *16*). Atomic emission instruments have only seldom used PDAs, since the number of detecting elements, or pixels, is much lower than the required resolution (*17*, *18*). There have been efforts to achieve high resolution with a limited number of PDA pixels, by prefiltering the spectrum and overlapping many orders (*19*, *20*). Several groups have made use of the emission lines in the near-infrared region, since many lines of interest are close enough together to be analyzed simultaneously with a very large array (*21–25*). This advantage is at the expense of a restricted wavelength range, which is located far from some of the most sensitive atomic lines.

The PDA used here has been described (*26*). Removing the window extended the wavelength range into the vacuum ultraviolet (vacuum UV). The modified PDA has 100 000 dynamic range and good responsivity down to 160 nm.

The desired performance of an atomic emission detector for gas chromatography could not be achieved by existing spectrometer designs. Therefore, a novel spectrometer was developed incorporating a concave holographic grating with a PDA that can travel along a long flat focal plane, Figure 1.

A polychromator with many PDAs covering the entire focal plane, as has been reported (*27*), was considered. However, with the plasma light source used here, different elements require different reagent gases within the plasma (*2*). This requirement reduces the utility of a multiple PDA polychromator.

THEORY

Basic Spectral Measurements. In atomic emission spectroscopy, there are three basic measurements: wavelength, intensity, and line width. Dark signal subtraction and base-line subtraction are usually made before these measurements.

There can be several difficulties when using PDAs (*28*, *29*). If the line intensity is measured as the maximum signal on a pixel, the highest pixel signal with the PDA fixed in position may not be the maximum attainable. If wavelength is measured from the position of the pixel with maximum signal, there is an uncertainty of half of a pixel width (*30*). Algorithms will be described that avoid these problems.

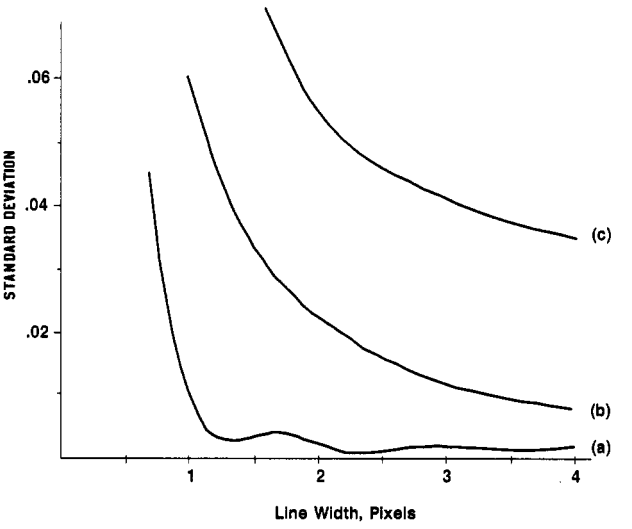

Figure 2. Calculated standard deviation of various line-center measurements, averaged over four line shapes, versus line width: (a) center of gravity algorithm; (b) median algorithm; (c) parabolic fit to peak maximum.

Wavelength calculation of a line depends on the physical position of the PDA and the measured line center relative to the pixels of the PDA. For accurate wavelength calibration, the line center must be precisely known to within a small fraction of a pixel, even though atomic lines are only a few pixels wide.

If a line is much narrower than the pixel width, the line center precision is limited to the pixel width. But if the line overlays several pixels and has a smooth shape, then the line center can be estimated much more precisely.

To locate line centers on an array, a parabolic fit to three or more signals spanning the top of a peak can give an estimate of the maximum (*31*, *32*). McGeorge and Salin achieved precisions of one-tenth of a pixel with a polynomial fit (*33*). Taylor investigated a median measure, that is, the fractional pixel location that bisects the base-line-corrected line area (*34*).

A center of gravity calculation has been used in a nonspectroscopic application to find the center of an optical image (*35*). Here, the line center is the sum of the base-line-corrected pixel signals, S_i, weighted by the pixel numbers, i, with the sum divided by the line area

$$\text{center of gravity} = \sum iS_i / \sum S_i \qquad (1)$$

In this work, the center of gravity estimate was found to be superior to the other estimates. The various algorithms for the line center were tested with various theoretical line shapes. The responses for Gaussian, Lorentzian, triangular, and trapezoidal images were calculated as each was moved across the PDA pattern in steps of 0.05 pixel widths. The standard deviation was found for the calculated line center relative to the true line center.

Figure 2 shows the average of the standard deviations of the measured line center from the true value for the four shapes, plotted as a function of line width. Three different algorithms for line center were investigated. For each theoretical line shape, at all tested line widths, the center of gravity algorithm was the algorithm most independent of relative pixel position. Whenever the line width is somewhat larger than the pixel width, the center of gravity calculation gives a good estimate of line center.

The center of gravity algorithm was tested with several strong lines by successively shifting the physical position of

Table I. Results of Line Center Measurements (Center of Mass Calculation)

element	wavelength, nm	peak width, pixels	std dev of line center, pixels	std dev of line center, nm
C	193.0	1.28	0.0233	0.004 91
He	318.8	1.42	0.0574	0.010 25
He	388.9	1.59	0.0588	0.009 43
He	492.2	2.39	0.0230	0.003 09
He	501.6	1.82	0.0185	0.002 44
H	656.3	2.82	0.0195	0.001 85
He	667.8	2.52	0.0203	0.001 87
He	706.5	2.78	0.0121	0.001 01
He	728.1	2.96	0.0124	0.000 98
O (triplet)	777.4	5.70	0.0151	0.001 04
average			0.026	0.003 68

the PDA a small fraction of a pixel width, and calculating the wavelength. This test was sensitive not only to the precision of the mathematical algorithm but also to the precision of the wavelength drive motor, noise, and spectral interferences.

Table I shows the experimental standard deviations of the line center determinations. The results are not as good as were predicted by the simulation. This is mostly due to the finite precision of about 0.01 pixel standard deviation of the wavelength drive motor. Two lines, at 318 and 388 nm, are worse than the others. This is thought to be due to minor spectral interferences, which disturb the base-line calculation.

Intensity of spectral lines can be measured several ways (*29*, *34*, *36*). The maximum pixel signal varies rapidly with the pixel registration for narrow lines. Averaging several pixel signals gives a considerable improvement in precision. Some groups have used a parabolic fit over the top of the peak to get a better estimate of the peak height. And, finally, the base-line-corrected area is used here.

With tests similar to those used for line width, the base-line-corrected peak area was found to be a more precise estimator of signal intensity than the other algorithms.

Line width can be used to measure electron temperature and to indicate degree of focus. The most commonly used peak-width algorithm (full width at half maximum, fwhm) suffers from a dependence on the relative registration of the line with the pattern of pixels. A more precise measure is the standard deviation, σ, of the base-line-corrected pixel measurements across the peak. The line width is reported here in units of peak width (fwhm), equal to 2.355σ. The numerical factor 2.355 is the ratio of peak width to the standard deviation for a theoretical Gaussian peak.

Wavelength calibration uses a table of PDA positions for several standard emission lines. In this instrument, the spectrometer focus is also measured and stored in the calibration table.

Standards for wavelength calibration can be the lines emitted by an auxiliary light source, such as a mercury lamp (*12*). In instruments where the sample can be kept in the plasma for a controlled length of time, the analytical line itself can be used for wavelength calibration.

In GC–AES, compounds may spend less than a second in the plasma, so that it is not feasible to use analytical lines for calibration. Therefore the spectrometer must be aligned before the beginning of a chromatogram and remain aligned during the run.

The helium spectrum provides several narrow, intense lines suitable for wavelength standards. The auxiliary gas flows provide low amounts of carbon, nitrogen, hydrogen, or oxygen, which can also be used as wavelength calibration lines.

Interpolation between calibration lines must be accurate to better than one part per thousand. A polynomial fit is

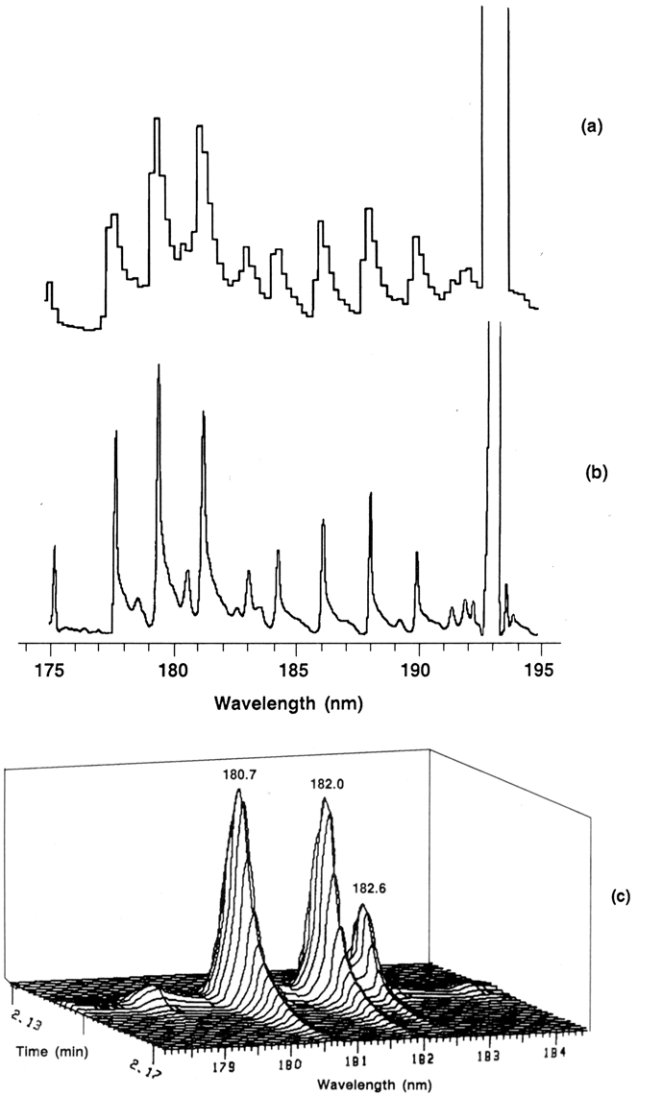

Figure 3. Spectral displays: (a) "snapshot"—real-time display taken during a hydrocarbon peak; (b) deconvolved scanned spectrum of the same region, with Aux reagent gas, off scale peak is carbon 193 nm; (c) three-dimensional display of snapshots, showing sulfur lines during a 4-ng peak of *tert*-dibutyl disulfide.

precise, but does not offer sufficient accuracy, since a polynomial is not the exact shape of the calibration curve. This problem is solved by converting mechanical position to nominal wavelength, using a numerical model of the spectrometer. Since nominal wavelength is very close to linear with actual wavelength, interpolation is sufficiently accurate.

Spectral Displays. Several different types of spectral output are shown in Figure 3. The primary spectral output of this system is a display of the pixel signals (Figure 3a), termed a "snapshot" to distinguish it from the spectrum. The snapshot is saved for each measurement cycle during a chromatogram (normally every 100 ms). Snapshots are used for confirming the presence of an element in a compound and for making new recipes (detection algorithms for an element).

When a classical spectrum is needed, the spectral resolution would normally be limited by the instrument resolution and the finite pixel width. This limitation can be largely overcome by the use of deconvolution and microstepping of the PDA. The position of the PDA is shifted in steps that are an integral fraction of the pixel width. The snapshots taken at each position are interleaved, giving a spectrum that is smoother than a single snapshot, but of similar resolution.

The image width of a microstepped spectrum is dominated by the width of the entrance slit and pixels. An increase in

resolution is made possible by deconvolving the contributions of the slit and pixel width, as shown in Figure 3b. The deconvolution reduces the spectral image width by a factor of approximately 3. A three-dimensional display of snapshots (Figure 3c) shows spectral features both by shape and by time variation. Figure 3c displays the spectra collected during the elution of 4 ng of sulfur as *tert*-butyl disulfide. The triplet is due to sulfur at 180.7, 182.0, and 182.6 nm. The same molecular spectrum shown in Figure 3a,b is also visible here.

Chromatographic Signal Processing. Signals specific for an element are produced by a "recipe", composed of a pair of linear functions of the various pixel signals. Each function is the scaler product, $\langle A,S \rangle$, of a filter, A, with the set of pixel responses, S, that is, the sum of weighting factors, A_i, multiplied by the corresponding pixel responses, S_i. For each spectral shape, S, there is an optimal filter, A, which depends on the noise characteristics.

The recipe for a particular element is composed of a response, $\langle E,S \rangle$, from an elemental filter, E, and a response, $\langle B,S \rangle$, from a filter for the background, B, according to the formula $\langle E,S \rangle - k\langle B,S \rangle$. The parameter k, termed the "background amount", determines how much background correction is performed. The background amount is adjusted to give optimal selectivity. The two time series, $\langle E,S \rangle$ and $\langle B,S \rangle$, are recorded separately. This allows the background amount to be changed after the data are recorded. In this way, the selectivity can be adjusted postrun.

At low elemental concentrations the noise level is nearly independent of the level of atomic emission. Under these conditions, the optimal element filter is the matched filter (*37*, *38*), where the coefficients A_i are equal to the base-line-corrected pixel responses for a noiseless spectrum of the desired element.

The elemental and background filters are made from snapshots of the desired spectral region collected during a chromatogram of a compound containing the element as well as compounds typical of interferences.

From the snapshot of the element, a portion is selected that contains the atomic line or lines of the element. This is used to create the signal filter, E. From a snapshot, M, of one of the interfering compounds, one or more segments are selected for the background filter, B. Figure 4 shows typical spectral fragments used to make a recipe for sulfur. Since filters are constructed from recorded snapshots, matched filters are automatically obtained.

Even if the PDA has not been moved since the recipes were made, the recipes are not generally located at the nominal wavelengths, due to thermal drift. Therefore, the recipes are shifted by a fraction of a pixel for proper alignment, prior to a chromatogram.

This software operation can be performed as a convolution of a shift filter with the original signal and background filters. The shifting operation can move the filters to any desired line center within the span of the PDA.

The shift filter is a three-term filter located at relative positions −1, 0, and 1 pixels. If the signal and background filters need to be shifted by an amount x, where x is between −0.5 and +0.5 pixel, then the coefficients of the shift filter are

$$\text{shift filter} = \frac{(x - 0.5)^2}{2}, \frac{3}{4} - x^2, \frac{(x + 0.5)^2}{2} \qquad (2)$$

This operation leaves the area of the signal and background filters unchanged but shifts their centers of gravity by x and increases their variances by 0.25 pixel^2.

The initial value of the background amount, k, is chosen so that the recipe is orthogonal to, or has null response to, the snapshot M

$$k = \langle E,M \rangle / \langle B,M \rangle \qquad (3)$$

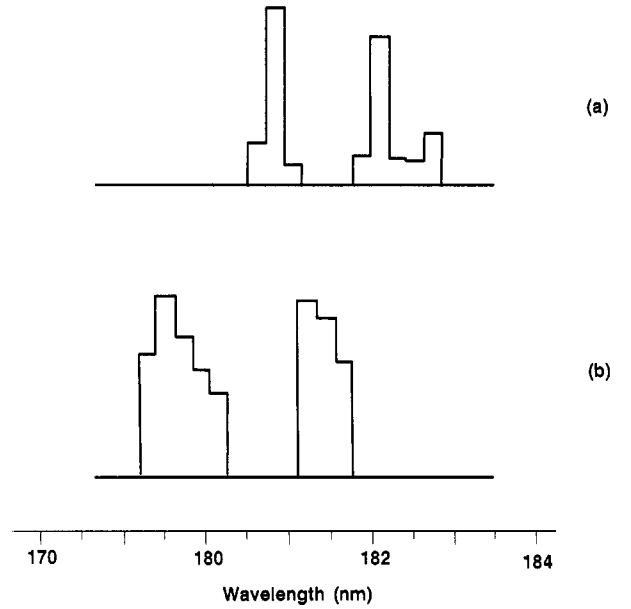

Figure 4. Fragments of snapshots from Figure 3, used to make a sulfur recipe: (a) signal, (b) background.

A more precise value of k, and therefore better selectivity, can be determined after a chromatogram is run.

After a chromatogram using a new recipe has been made, a portion of it is selected, which contains only compounds free of the element of interest. The background amount can be adjusted to minimize chromatographic response within this time span, either by iterative means or by variational methods.

Parts a and b of Figure 5 show the signal and background chromatograms of a test mixture made with a sulfur recipe. The test mixture contains *tert*-butyl disulfide, several hydrocarbons, octane, tridecane, tetradecane, and an excess of dodecane. A region including the tridecane peak is used in optimizing the background amount. Once the background amount is set, a chromatogram results (Figure 5c), which has no visible response from C13 and C14 and very small response from C8 and C12. The remaining small peaks are sulfur impurities, as confirmed by their snapshots.

Doubly Orthogonal Recipes. In some cases, there is more than one interfering molecular band or the structure of the band changes at very high sample concentrations. This is the case for C8 and C12 in Figure 5c. One symptom of this is a large interfering peak requiring a different background amount for its response to be minimized, compared to a small interferant of the same type. What is needed is a type of recipe which is doubly orthogonal, that is, which has null response to two different background spectra.

The structure of a doubly orthogonal recipe is a generalization of the simpler recipes discussed so far. A doubly orthogonal recipe has a signal filter E, but the background filter is split into two parts, B and C, which have separate background amounts, k and j, respectively. The recipe has three parts

$$= E - kB - jC \qquad (4)$$

Under what circumstances will this recipe be orthogonal to two interfering spectra, as represented by snapshots M and N?

$$\langle E,M \rangle - k\langle B,M \rangle - j\langle C,M \rangle = 0 \qquad (5)$$

and

$$\langle E,N \rangle - k\langle B,N \rangle - j\langle C,N \rangle = 0 \qquad (6)$$

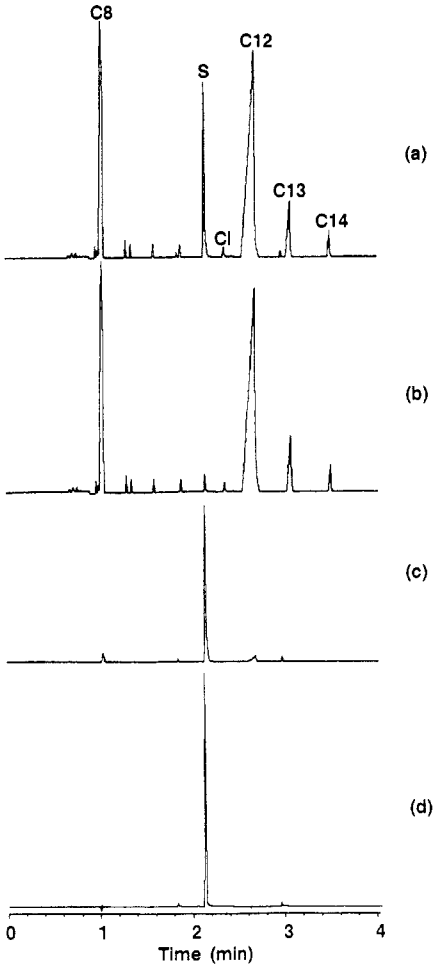

Figure 5. Chromatogram from sulfur recipe, and its constituent parts: (a) element filter, E; (b) background filter, B; (c) the resultant chromatogram, equal to the combination $E-kB$, with background amount $k = 0.9773$; (d) chromatogram made with doubly orthogonal recipe. Labeled compounds are as follows: C8, 790 ng of *n*-octane; S, 10 ng of *tert*-dibutyl disulfide; Cl, 16 ng of 1,2,4-trichlorobenzene; C12, 840 ng of *n*-dodecane; C13, 85 ng of *n*-tridecane; and C14, 26 ng of *n*-tetradecane.

Solving simultaneously for the background amounts k and j

$$j = \frac{\langle B,M\rangle\langle E,N\rangle - \langle E,M\rangle\langle B,N\rangle}{\langle B,M\rangle\langle C,N\rangle - \langle C,M\rangle\langle B,N\rangle} \quad (7)$$

$$k = \frac{\langle C,N\rangle\langle E,M\rangle - \langle C,M\rangle\langle E,N\rangle}{\langle B,M\rangle\langle C,N\rangle - \langle C,M\rangle\langle B,N\rangle} \quad (8)$$

When background filters B and C are selected, it is not generally obvious whether the coefficients k and j will be positive. In some cases, the great majority of arbitrary choices of background filters give a negative value for either k or j. Positive values are preferred, to prevent the two parts of the background from partially cancelling each other.

An algorithm to do this categorizes all pixels neighboring the signal filter E into two groups: those responding relatively more to the M snapshot, and those responding more to the N snapshot. For this calculation, the response of the signal filter E to each of the snapshots M and N must also be taken into consideration.

It can be shown algebraically that if the filter B contains components only at pixels in the first group and that the C filter contains only components at pixels in the other group, that the two background amounts k and j will always be positive.

This calculation works in the following way. Three snapshots are collected during a chromatogram, representing the spectrum of an element of interest, and two interfering spectra, M and N. The elemental filter E is formed in the usual way. At this point, the above-mentioned algorithm partitions the pixels into those suitable for a filter based on the M snapshot and those suitable for one based on the N snapshot. The unsuitable pixel signals are set to zero in the M and N snapshots. When these modified snapshots are used to select the background, the result is guaranteed to have positive values of k and j in eqs 7 and 8.

Figure 5d shows the output of a doubly orthogonal sulfur recipe. The recipe was made by using snapshots from C13 and C8. The selectivity to C12 has improved by a factor of 5.

EXPERIMENTAL SECTION

A prototype Hewlett-Packard 5921A atomic emission detector was used. This was coupled with an HP 5890A gas chromatograph, and an HP 7673A automatic injector controlled by a HP 330 computer with HP 35920A GC/AED software. Computer peripherals included a DMA card, high-speed HP-IB disk interface, an HP PaintJet color printer, and an HP 7550A (eight-pen) plotter. An Eventide Model WPB-109 "print buffer" was used to free the computer from waiting for output to print or plot.

Light Source. The atomic emission is produced by a helium plasma within a reentrant microwave cavity. The plasma is contained within a 1 mm i.d. silica tube, which is viewed axially. Many of the improvements in performance are due to the low temperature of the discharge tube walls. The water cooling and the 0.12 mm tube wall thickness give a wall temperature estimated at 350 °C.

The plasma discharge apparatus, as well as the microwave power supply, heated transfer line, and gas flow system have been described in a companion paper in this issue (*2*).

Spectrometer. A concave grating mount was chosen for the spectrometer, since it has a minimal number of optical elements.

A concave holographic grating can be made with a flat focal plane (*39, 40*). For the resolution needed here, a long focal plane was used, with provision to move the PDA along the focal plane.

Figure 1 shows the schematic diagram of the spectrometer. The spectrometer has some of the aspects of a polychromator, in that many lines clustered within the width of the PDA can be measured simultaneously. But it also has features of a monochromator: the spectrometer can be set at any wavelength and it can scan a continuous spectrum. Because of this dichotomy, perhaps a different term, such as "oligochromator", should be used.

Wavelength precision and accuracy are affected by thermal control and by the frequency of wavelength calibration or correction. Wavelength correction occurs at the beginning of each chromatographic run, so that only thermal drifts occurring during the time span of a single run can have any effect. The spectrometer is in close thermal contact with a massive aluminum plate, and the exterior of the spectrometer is heavily thermally insulated. This results in a thermal time-constant in excess of 20 h.

For optimal sensitivity, the most sensitive atomic lines should be used for the major elements of interest. The sensitivity advantages of the vacuum ultraviolet region (vacuum UV) for elements such as C, S, and N have been reported (*41–43*). There has also been work in the near-infrared region (near-IR) with PDAs (*22–25*), as well as with interferometers (*4–6*). The vacuum UV region is many times more sensitive for elements such as carbon, nitrogen, sulfur, and phosphorus. However, the near-IR region has uniquely sensitive lines for oxygen and fluorine. Thus, an unusually wide wavelength range, 160–800 nm, was selected.

Resolution was chosen to resolve the nearest pair of analytical lines, hydrogen and deuterium at 656 nm, which are separated by 0.18 nm. A higher resolution was not used, so that several sets of neighboring atomic lines could be measured simultaneously, such as the C, H, Cl, and Br lines near 480 nm, and the C, N, and S lines near 180 nm.

Table II. Spectrometer Components and Operating Conditions

focal length	0.3 m
f/number	*f*/3.6
focal plane length	0.35 m
grating groove density	550/mm
grating groove depth	0.08 μm
wavelength range	160–800 nm
dispersion	0.2 (vacuum UV) to 0.06 (near-IR) nm/pixel
resolution	0.1 nm at 400 nm
entrance slit width	0.05 mm
purge gas	nitrogen
order sorters UV	280 nm
Vis	460 nm
condensing optics	90° elliptical mirror
	0.13 m focal length
detector	211 pixel photodiode array
pixel size	0.6 × 0.006 mm
dark current	0.5 pA at 25 °C
dynamic range	10^5

The groove profile of the diffraction grating determines the wavelength range and maximum grating efficiency. A sinusiodal groove profile was used to achieve the needed 5:1 wavelength range. With this profile, the maximum grating efficiency is lower by a factor of 3 compared to an ideal blazed grating. The wavelength of maximum efficiency was set midway between the vacuum UV and the visible by selection of a groove depth of 0.08 μm.

The properties of the concave grating spectrometer are described in Table II. The cavity is attached to the outside wall of the spectrometer, so that the focal point of the elliptical mirror is 2 mm into the end of the discharge tube. The plane of the spectrometer is arranged vertically, to minimize the area on the laboratory bench occupied by the instrument.

When the PDA is moved along the focal plane, the line of travel deviates slightly from the true focal plane. Better performance is achieved by adjusting the focus automatically at each wavelength, by moving the entrance slit toward or away from the grating.

Photodiode Array. The optical detector is a photodiode array with response down to 160 nm. The readout rate is usually 10 Hz, although 100 Hz is sometimes used during calibration routines.

The noise of the PDA measurement was measured during the response of the 193-nm carbon line. Normally, measurements are made on a single pixel to characterize the noise. Here, however, the base-line-corrected area is used, since it more closely models typical measurement methods. The standard deviation of the response was used as an indicator of the noise.

The line intensity was varied over its entire dynamic range, which was in excess of 100 000. Only two sources were found to make significant contributions to the noise: the shot noise of the continuum and the flicker noise of the source. The latter is estimated to contribute a standard deviation that is 2000 times lower than the measured area.

Gas Chromatographic Conditions. The column used was a fused silica WCOT column, 25 m long × 0.32 mm i.d., with a 0.17 μm film thickness of HP-1, which is a cross-linked methyl silicone. The carrier gas was helium at 28 cm/s linear velocity. The transfer line has temperature setpoints at the GC end, at the line itself, and at the microwave cavity. Each was set to 250 °C. The column extends out of the oven, through the transfer line, into the discharge tube. Thus, approximately 0.6 m of the column is operated isothermally at 250 °C. The injection port was 250 °C; the oven program was 40 to 220 °C at 20 °C/min. The injection was split mode, with a split ratio of 36:1.

For the precision measurements, automated on-column injection into a 30 m long × 0.53 mm i.d. column coated with a 0.88 μm thick film of HP-1 was used. The temperature program was initially at 60 °C for 2 min, then 20 °C/min to 200 °C.

Materials. Isooctane was obtained from Burdick and Jackson (Muskegon, MI). The remainder of the sample reagents were obtained from Aldrich (Milwaukee, WI).

Gases were research grade (except for the nitrogen used for purging the spectrometer) and were purchased from Air Products (Allentown, PA). The helium was purified further by passing it through a heated getter obtained from SAES Getters (Colorado Springs, CO).

Table III. Changes in Sensitivity and Selectivity with a 0.025-nm Wavelength Shift[a]

element	sensitivity, %	selectivity, %
chlorine	4.15	31.5
bromine	2.44	69.3
sulfur	2.90	20.9
nitrogen	2.58	23.2

[a] Averaged over positive and negative wavelength shifts and over measurements on six instruments.

RESULTS

The previous paper (2) described the limits of detection and the selectivity of the AED. The remainder of this paper will emphasize the precision and recipe optimization aspects of the technique.

Chromatographic Precision. Two main sources of imprecision in quantitative measurements are errors in setting the wavelength and wavelength drift of the spectrometer.

Wavelength setting errors were evaluated by moving the PDA to a series of emission lines of known wavelength and comparing the specified wavelengths with the measured ones. The test included six of the calibration lines, listed in Table I, and also six uncalibrated lines. The test was done by using three different AED instruments. For the six calibration lines, the root mean square error averaged over all of the wavelengths and instruments was 0.0082 nm. No significant error in wavelength interpolation was found, since the uncalibrated lines had nearly the same error: 0.0079 nm.

An error of 0.008 nm would have a measurable effect on chromatographic precision. For this reason, the alignment of recipes prior to the GC run uses a more precise method. A known line that is close to the recipes is aligned exactly with the center of a pixel. This line is then used as a wavelength standard for locating the recipes on the PDA.

This approach circumvents errors due to motor movements, errors in the calibration table, and errors in interpolation. The only major remaining error possibility is that of measuring the line center. As Table I shows, this error is lower by approximately a factor of 2.

What is the effect on sensitivity and selectivity of wavelength errors? A series of recipes for Cl, Br, S, and N were made with the wavelength shifted by +0.025 nm and by −0.025 nm, which is 6 times larger than the expected wavelength error. The eight new recipes, along with the four original recipes, were run on six different instruments. The spectrometer can run as many as eight recipes simultaneously, so the six chlorine and bromine recipes were run together. The nitrogen and sulfur recipes were run in a second injection.

The results are summarized in Table III. The sensitivities, expressed as minimum detectable levels, only vary by a few percent. There are much larger variations in selectivity. Selectivity theoretically goes to infinity at a wavelength where the interfering response changes from positive to negative. Therefore, small wavelength errors give large fractional changes in selectivity.

To resolve the difficulties of measuring selectivity, a more stringent criterion than usual was employed. The background amount was optimized by minimizing the interfering response to a small hydrocarbon peak, but selectivity was measured by using a much larger hydrocarbon peak. In this case, selectivity is not infinite, since the interfering response is more easily measured with the larger peak, and there is often a slight difference in optimal background amount for different peaks.

The bromine recipe has greater sensitivity to wavelength

Table IV. Precisions of Chromatographic Areas over Many Injections

line	compounds	% relative standard deviations	
		50 injections	5 injections
C 193 nm	*a*	1.09–1.27	0.34–0.51
C 496 nm[b]	*a*	0.95–1.05	0.32–0.44
H 486 nm	*a*	0.65–1.52	0.51–1.35
Br 478 nm	bromohexane	1.22	0.61
S 181 nm	*tert*-butyl disulfide	3.53	1.37
Cl 479 nm	trichlorobenzene	1.03	0.62

[a] Compounds: fluoroanisole, bromohexane, *tert*-butyl disulfide, *n*-dodecane, and *n*-eicosane. [b] Second order of C 247.9 nm.

errors than the other recipes. Since chlorine and bromine have similar spectral behavior, the difference between the performance of the two recipes is not completely understood. Work is continuing on the development of recipes that are more resistant to wavelength errors.

So far, the test results reported have been aimed at a few specific error terms. Performance was also measured under more normal operating conditions. An automated method to run a standard test mixture 50 times in succession was constructed. The test ran for approximately 60 h, during which the ambient temperature varied diurnally by approximately 5 °C. Each run consisted of two on-column injections, one to measure C, H, Cl, and Br in the visible region, and the other to measure C and S in the vacuum UV. Each compound in the standard was present at the 4–8-ng level. Table IV shows the precision of the measured areas for each peak.

The common elements, carbon and hydrogen, were measured for five compounds. Over any subset of five consecutive injections, the standard deviations for each area measurement of each compound were near 0.5%, with hydrogen being slightly worse than carbon. When all 50 injections were used for calculations, the standard deviations were a factor of 2 to 3 higher, since slow variations in measured areas had a larger effect.

The data for bromine and chlorine detection are similar, but the variation is larger for sulfur. Similar results had been seen earlier for nitrogen at 174 nm. This was traced to an inadequate spectrometer purge flow, which allowed a small amount of ambient air to enter the spectrometer. When similar tests were run after the problem was corrected, the area measurements of sulfur were more stable.

Optimizing Recipes. Chlorine and bromine recipes can be made in the region between 460 and 490 nm, since each element has a strong triplet of ionic emission lines there. There is also a hydrogen line and several possibilities for carbon detection either in or just outside the region. Recipes have been developed for all of these elements, but only the chlorine and bromine work is reported here. A report on detection of carbon and hydrogen has been published previously (*44*).

Since recipes are made from spectra, the first step in developing new recipes is investigating the spectra near the atomic lines under various conditions. Certain regions of these spectra are chosen for recipe making, while other regions with complicated interferences are best avoided.

Figure 6 shows several snapshots between 460 and 490 nm. Atomic lines were identified with the help of Zaidel et al. (*45*). Molecular bands were identified by using the tables of Pearse and Gaydon (*46*).

Figure 6a was taken with only helium in the plasma—no reagent gases or compounds eluting. The hydrogen 486.1-nm line is due to impurities in the helium supply, estimated to be approximately 500 pg/mL of hydrogen. The figure shows both a helium atomic emission line at 471.7 nm and molecular

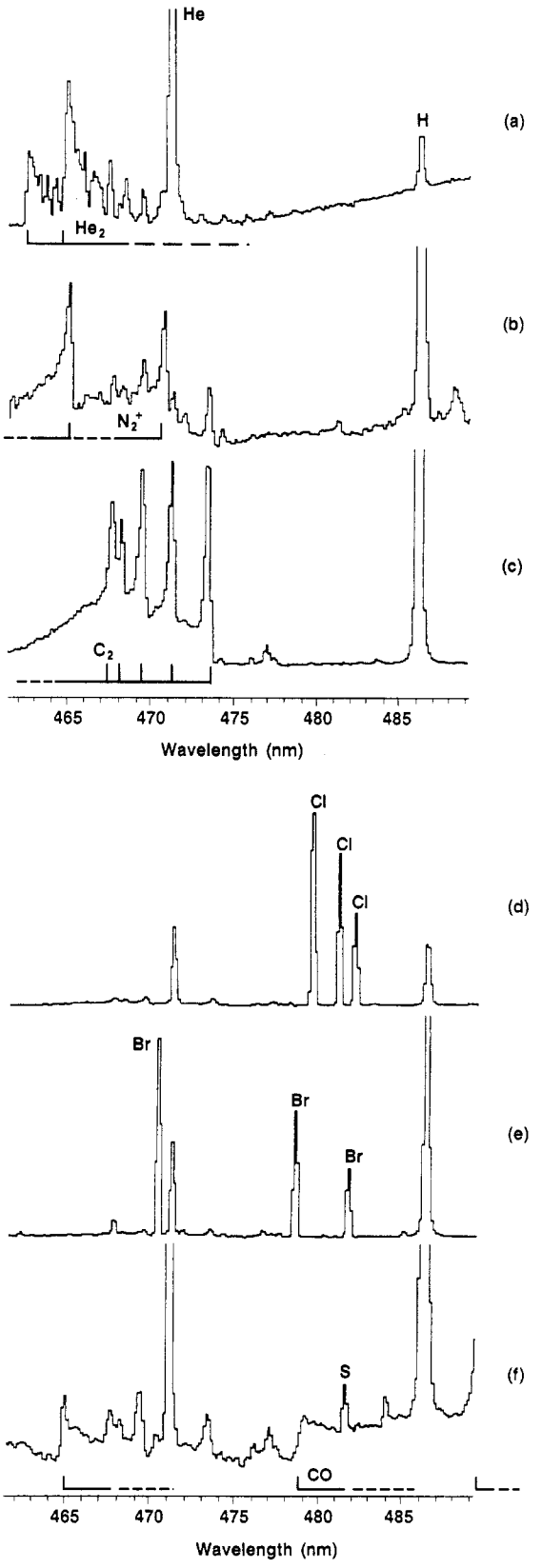

Figure 6. Snapshots in the 475-nm region; oxygen reagent gas and UV order sorter unless noted: (a) no reagent gas; (b) "Aux" reagent gas; (c) during elution of 840 ng of dodecane; (d) during elution of 16 ng of trichlorobenzene; (e) during elution of 13 ng of 1-bromohexane; (f) during elution of 10 ng of *tert*-butyl disulfide with no order-sorting filter.

emission due to He_2, with two band heads at 462.6 and 464.8 nm. The molecular helium bands were not found to interfere with measurements, since they are quenched by any of the reagent gases. With the reagent gases turned off, the helium

bands indicate that there are no gross contaminants in the helium flow.

Figure 6b shows a snapshot with the Aux reagent gas (10% methane in nitrogen). The two band heads at 465.2 nm and 470.9 nm in Figure 6b are due to the first negative system of N_2^+. During runs with oxygen reagent gas, which is more commonly used in this spectral region, organic compounds containing nitrogen did not show these N_2^+ bands. This is probably because nitrogen is more likely to be found in the atomic state, or present as CN or NO. However, N_2^+ bands were found during large air leaks.

Figure 6c shows a snapshot taken during the elution of 840 ng of dodecane, with oxygen reagent gas. There are five major bands of the Swan system of C_2, at 467.9, 468.5, 469.8, 471.5, and 473.7 nm. The bands are evident during the elution of nearly all organic compounds at levels of more than a few nanograms. In fact, there are traces of these bands evident in Figure 6b,f. These bands are not generally useful for quantitative measurement of carbon, since the response is not linear; better carbon results are found by using the second-order atomic carbon line at 495.7 nm.

Figure 6d,e shows the ionic lines for chlorine and bromine. These snapshots were taken during the elution of 16 ng of trichlorobenzene and 10 ng of 1-bromohexane, respectively. One chlorine line and two bromine lines show potential overlaps with other spectral features, so that only the middle bromine line at 478.6 nm, and the two larger chlorine lines at 479.5 nm and 481.0 nm, should be used to make recipes.

Figure 6f was taken during the elution of 10 ng of *tert*-butyl disulfide, without the presence of the UV order sorting filter. The absence of the filter allows the transmission of some additional bands in the second order. These are probably due to the fourth positive system of CO and/or the first negative system of CO^+ (47). Several of the C_2 bands that were seen in Figure 6c are present here at low levels. A small atomic line of sulfur, 481.5 nm, is visible; it overlaps the smallest lines of both the chlorine and the bromine triplets. These two lines should not be used in recipes, because of interferences with sulfur-containing compounds.

Consider the construction of a chlorine recipe. The signal filter should include one or both of the two larger chlorine lines in Figure 6d. A region of the snapshot should be selected to compensate for background interferences such as those shown in Figure 6f. A randomly selected background region not affected by atomic interferences will usually give good results, once the background amount is set correctly. But much better selectivity can be achieved, if a doubly orthogonal recipe is used.

The background near the chlorine triplet is more easily seen with hydrocarbon snapshots of the spectral region. Figure 7a shows a three-dimensional display taken during the elution of 26 ng of tetradecane. There are bands present in the base line that are suppressed while the peak elutes. The snapshots during the peak are mostly continuum-like, with a few spectral features superimposed. These spectral features are different from those seen during the base line.

When a much larger hydrocarbon concentration is present, the detailed shape of the background changes. Figure 7b was taken during the elution of 840 ng of dodecane, at a much higher concentration than that of tetradecane in Figure 7a. It also appears to be mostly continuum-like, with some structure evident. However, the details of the structure are different from that shown in Figure 7a.

If the background spectrum contained only a single feature, which was linear with sample concentration, then correction by subtracting a constant fraction of the background signal would work perfectly. But, as has been shown, background is nonlinear; different spectral features dominate at different

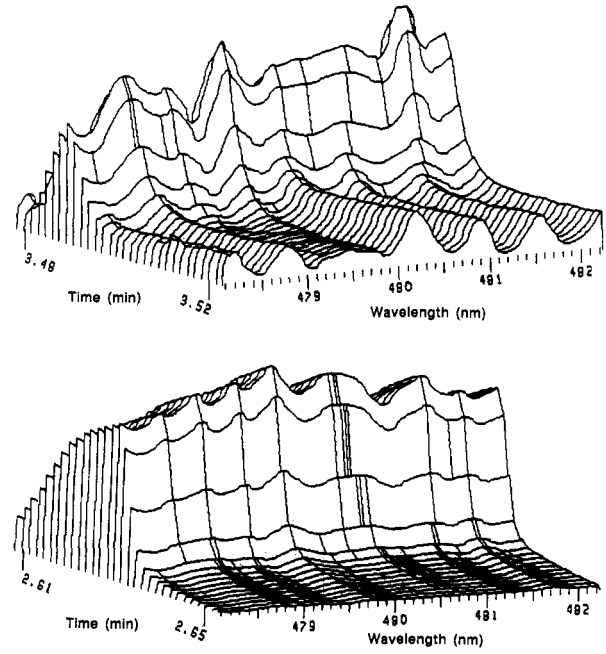

Figure 7. Three-dimensional display of snapshots during elution of different amounts of hydrocarbons: (a) 26 ng of tetradecane, (b) 840 ng of dodecane.

concentrations. In chromatography, the result is variation of the optimal value of background amount with concentration. For instance, for one chlorine recipe with a singly orthogonal background filter, the background amounts that null the hydrocarbon response shown in parts a and b of Figure 7 are 0.73 and 1.02, respectively.

A doubly orthogonal recipe was made, using Figure 6d to make the signal filter, and Figure 7a,b to make the background filters. Since three interfering bands are present, a triply orthogonal recipe was considered, but found not to be necessary, since the base-line bands in Figure 7 are only present at low levels of compound, where the lower signal to noise ratio makes a higher degree of base-line correction unnecessary. The doubly orthogonal recipe was compared to a singly orthogonal recipe, as well as three simpler filters. The same sample shown in Figure 5 was used for this test.

Recipes had their background amounts adjusted to minimize the response to tridecane. Selectivity was measured versus tridecane itself, and also versus octane, which was present at much higher concentrations. Minimum detectable level was calculated as that concentration giving a signal to noise ratio of 2, with noise taken as 6 times the root mean square deviation of a length of base line.

Table V shows results averaged over 10 chromatograms. A recipe made of a single pixel offers poor selectivity. It would be somewhat better if an order-sorting filter were used to suppress the interfering bands from carbon monoxide, but this would have negated the ability to make simultaneous chromatograms of carbon. Adding two background correction pixels with a background amount of 0.5 should correct for a background which varies slowly with wavelength. Here, however, the background is not slowly varying so there is little improvement in selectivity. Good selectivity is achieved only if the background amount is set precisely. Now, however, the minimum detectable level is degraded, since the noise contributions from the background pixels are increased.

The fourth recipe in Table V is a matched recipe of the singly orthogonal type, matched to the largest chlorine line. The background filter was made from a hydrocarbon snapshot and has two parts on either side of the chlorine line.

This singly orthogonal recipe exhibits both improved sensitivity and selectivity versus tridecane. However, the different

Table V. Minimum Detectable Level (MDL) and Molar Selectivities for Various Chlorine Recipes[a]

recipe		background amount		MDL		selectivity × 1000			
signal	background	av	% σ	pg/s	% σ	vs C13	% σ	vs C8	% σ
1 pixel				25.1	8.8	0.30	3.1	0.13	1.8
1 pixel	2 pixels	0.5000		25.7	10.0	0.51	3.1	0.24	2.1
1 pixel	2 pixels	1.2144	0.33	32.0	10.8	8.05	5.5	1.09	3.4
matched	singly ortho	0.8671	0.20	23.6	8.9	11.65	9.2	0.93	2.0
matched	doubly ortho	0.9864	0.18	22.9	5.2	24.68	13.3	12.46	13.9

[a] Averaged over 10 injections.

Table VI. Variation of Molar Selectivity among Six Instruments

recipe	av MDL, pg/s	selectivity × 1000					
		versus C13			versus C8		
		min	max	av	min	max	av
Cl single	23.47	8.01	46.16	21.60	1.03	4.81	2.60
Cl double	20.76	12.74	45.29	29.87	8.44	53.47	23.59
Br single	12.96	7.34	26.04	11.19	0.94	13.97	5.05
Br double	15.96	12.45	21.92	19.35	4.61	24.18	12.76

spectral structure of the larger octane peak shows no improved selectivity.

The last recipe in Table V is doubly orthogonal. As expected, the selectivity measured with respect to larger hydrocarbon peaks such as octane was improved; but the selectivity with respect to tridecane was also improved. This is because there are slight changes in the spectral structure between the top of a peak and its base, even for a small peak like tridecane. While the background amount can be adjusted to null the response at the top of the peak, this difference causes small excursions at the beginning and/or end of the peak. This problem is greatly reduced by using doubly orthogonal recipes.

Surprisingly, the more "highly tuned" recipes have not always been found to be the most sensitive to variation from run to run. Table V shows the relative standard deviation for the background amount, MDL and the two measurements of selectivity. The doubly orthogonal recipe has the lowest standard deviation for background amount and MDL. It also has the largest relative standard deviation for selectivity, but this is because its interferences are approaching zero.

It might be expected that recipes made on one instrument might not perform as well on others, due to differences in the plasma or spectrometer. The singly and doubly orthogonal recipes developed for chlorine were used on a total of six instruments, and the same test was performed. Bromine recipes of both types were also run on the six instruments. See Table VI.

The doubly orthogonal chlorine recipe had octane selectivities ranging from 8440 up to 53 500. On every instrument, both doubly orthogonal recipes had better selectivity than their singly orthogonal counterparts, both with respect to tridecane and with respect to octane. On average, the selectivities were similar or slightly better than those on the instrument on which the recipes were made. This original instrument had the fourth-highest selectivity for chlorine, and the second highest for bromine, of the six instruments. These results indicate that recipes can be copied from one instrument to another, while preserving high selectivity.

CONCLUSION

A PDA-based spectrometer has been developed for multielement analysis using GC–AES. The objectives of good sensitivity, selectivity, and suitability for unattended operation have been addressed.

Sensitivity has been improved by means of high optical throughput, low noise levels in the detector, and the use of sensitive emission lines in the vacuum UV. The PDA can be used with digital filters matched to the shape of the emission line. This also enhances the sensitivity, as demonstrated in Table V for chlorine.

Selectivities have been investigated for sulfur, chlorine, and bromine. As shown in the previous paper (*2*), these exceed selectivities previously reported by a large factor. This improvement is due to the PDAs ability to perform real-time multipoint background correction. The signal processing method, or recipe, separates the measurement of background and signal, allowing a convenient and precise method of adjusting selectivity after the completion of the chromatogram. This is seen as more than a convenience factor, since the background correction can be performed more accurately, and it can be optimized successively with respect to several different interfering compounds.

Even with the real-time, multipoint background correction provided by a PDA, there are still cases of noticeable interference. Snapshots, which are spectra collected during the chromatogram, have shown that this interference is caused by changes in an interfering spectral component with concentration. A doubly orthogonal recipe structure has been developed, which improves the selectivity still further.

Unattended operation requires the ability to handle ambient variations such as temperature and to provide high sensitivity and selectivity over a long period of time. The performance of the system has been tested against wavelength errors, especially due to temperature drift. The reproducibility of the analytical results over time has been found to be very good, with responses varying by typically 1% over several days. The system has been shown to provide high-quality analytical results, even when recipes are shared between many different instruments.

It is concluded that this technique is sufficiently sensitive and stable for general analytical use as a multielement GC detector. It is the judgment of the authors that it represents the closest approach yet to the ideal elemental detector described by LaFreniere, Fassel, and Eckels (*1*).

ACKNOWLEDGMENT

The authors wish to thank Paul Dryden for designing the performance tests on six instruments. In addition, thanks are due to Len Bilen, Steve Craig, Bill Hewlett, George Hudak, Keith Knauss, Dick Kolloff, Chuck Masters, Andy Murphy, Dave Packard, Tom Przybylski, Bob Rhodes, Dan Smisko, George Walsh, Andy Warchol, and Barry Willis for their efforts, without which this work would not have been possible.

LITERATURE CITED

(1) LaFreniere, K. E.; Fassel, V. A.; Eckels, D. E. *Anal. Chem.* **1987**, *59*, 879–887.
(2) Quimby, B. D.; Sullivan, J. J. *Anal. Chem.*, preceding paper in this issue.
(3) Quimby, B. D.; Uden, P. C.; Barnes, R. M. *Anal. Chem.* **1978**, *50*, 2112–2118.
(4) Hubert, J.; Van Tra, H.; Tran, K. C.; Baudais, F. L. *Appl. Spectrosc.* **1986**, *40*, 759–766.

(5) Pivonka, D. E.; Fateley, W. G.; Fry, R. C. *Appl. Spectrosc.* **1986**, *40*, 291-297.
(6) Pivonka, D. E.; Schleisman, A. J. J.; Fateley, W. G.; Fry, R. C. *Appl. Spectrosc.* **1986**, *40*, 766-772.
(7) Cerbus, C. S.; Gluck, S. J. *Spectrochim. Acta* **1983**, *38B*, 387-397.
(8) Goode, S. R.; Kimbrough, L. K. *Spectrochim. Acta* **1987**, *42B*, 309-322.
(9) Eckhoff, M. A.; Ridgway, T. H.; Caruso, J. A. *Anal. Chem.* **1983**, *55*, 1004-1009.
(10) Holcombe, J. A.; Harnly, J. M. *Anal. Chem.* **1986**, *58*, 2606-2611.
(11) de Galan, L.; Kornblum, G. R.; de Loos-Vollebregt, M. T. C. *Recent Advances in Analytical Spectroscopy*; Fuwa, K., Ed.; Pergamon: New York, 1982; pp 33-50.
(12) Olesik, J. W. *Inductively Coupled Plasma Emission Spectroscopy*; Boumans, P. W. J. M., Ed.; Wiley-Interscience: New York, 1987; Part 1, pp 466-535.
(13) Haas, D. L.; Caruso, J. A. *Anal. Chem.* **1985**, *57*, 846-851.
(14) Talmi, Y.; Simpson, R. W. *Appl. Opt.* **1980**, *19*, 1401-1414.
(15) Jones, D. G. *Anal. Chem.* **1985**, *57*, 1057A-1073A and 1207A-1214A.
(16) Borman, S. A. *Anal. Chem.* **1983**, *55*, 836A-842A.
(17) Blades, M. W.; Horlick, G. *Appl. Spectrosc.* **1980**, *34*, 696-699.
(18) Choot, E. H.; Horlick, G. *Spectrochim. Acta* **1986**, *41B*, 935-945.
(19) Levy, G. M.; Quaglia, A.; Lazure, R. E.; McGeorge, S. W. *Spectrochim. Acta* **1987**, *42B*, 341-351.
(20) Karanassios, V.; Horlick, G. *Appl. Spectrosc.* **1986**, *40*, 813-821.
(21) Freeman, J. E.; Hieftje, G. M. *Spectrochim. Acta* **1985**, *40B*, 475-492.
(22) Keane, J. M.; Brown, D. C.; Fry, R. C. *Anal. Chem.* **1985**, *57*, 2526-2533.
(23) Keane, J. M.; Fry, R. C. *Anal. Chem.* **1986**, *58*, 790-797.
(24) Chan, S.; Montaser, A. *Appl. Spectrosc.* **1987**, *41*, 545-552.
(25) Takigawa, Y.; Hanai, T.; Hubert, J. *HRC CC, J. High Resolut. Chromatogr. Chromatogr. Commun.* **1986**, *9*, 698-702.
(26) Kamins, T. I.; Fong, G. T. *IEEE J. Solid-State Circuits* **1978**, *SC-13*, 80-85.
(27) Brett, L.; Stahl, R. G.; Timmins, K. J. *J. Anal. At. Spectrom.* **1989**, *4*, 333-336.
(28) Burton, L. L.; Blades, M. W. *Spectrochim. Acta* **1987**, *42B*, 513-519.
(29) Winge, R. K.; Fassel, V. A.; Eckels, D. E. *Appl. Spectrosc.* **1986**, *40*, 461-464.
(30) Grabau, F.; Talmi, Y. *Multichannel Image Detectors*; ACS Monograph Series No. 236; Talmi, Y., Ed.; American Chemical Society: Washington, DC, 1983; Volume 2, pp 75-116.
(31) McGeorge, S. W.; Salin, E. D. *Anal. Chem.* **1985**, *57*, 2740-2743.
(32) Kempster, P. L.; Strasheim, A.; Bohmer, R. G. *Spectrochim. Acta* **1987**, *42B*, 1139-1143.
(33) McGeorge, S. W.; Salin, E. D. *Spectrochim. Acta* **1986**, *41B*, 327-333.
(34) Taylor, P.; Schutyser, P. *Spectrochim. Acta* **1986**, *41B*, 81-103.
(35) Stewart, J. A.; Scheeline, A. *Anal. Chem.* **1984**, *56*, 2995-2997.
(36) van der Plas, P. S. C.; Uitbeijerse, E.; de Loos-Vollebregt, M. T. C.; de Galan, L. *Spectrochim. Acta* **1987**, *42B*, 1027-1038.
(37) Hirschfeld, T. *Appl. Spectrosc.* **1976**, *30*, 67-68.
(38) Bialkowski, S. E. *Appl. Spectrosc.* **1988**, *42*, 807-811.
(39) Cordelle, J.; Flamand, J.; Pieuchard, G.; Labeyrie, A. *Optical Instruments and Techniques 1969*; Dickson, J. Home, Ed.; Oriel Press: Newcastle, 1970; pp 117-124.
(40) Noda, H.; Namioka, T.; Seya, M. *J. Opt. Soc. Am.* **1974**, *64*, 1031-1048.
(41) Braun, W.; Peterson, N. C.; Bass, A. M.; Kurylo, M. J. *J. Chromatogr.* **1971**, *55*, 237-248.
(42) Uehiro, T.; Morita, M.; Fuwa, K. *Anal. Chem.* **1984**, *56*, 2020-2024.
(43) LaFreniere, B. R.; Houk, R. S.; Wiederin, D. R.; Fassel, V. A. *Anal. Chem.* **1988**, *60*, 23-26.
(44) Sullivan, J. J.; Quimby, B. D. *HRC CC, J. High Resolut. Chromatogr. Chromatogr. Commun.* **1989**, *12*, 282-286.
(45) Zaidel', A. N.; Prokof'ev, V. K.; Raiskii, S. M.; Slavnyi, V. A.; Shreider, E. Ya. *Tables of Spectral Lines*, IFI/Plenum: New York, 1970.
(46) Pearse, R. W. B.; Gaydon, A. G. *The Identification of Molecular Spectra*; Chapman & Hall: London, 1963.
(47) Krupenie, P. H. *The Band Spectrum of Carbon Monoxide*; National Standard Reference Data Series, National Bureau of Standards NSRDS-NBS 5; U.S. Government Printing Office: Washington, DC, 1966.

RECEIVED for review October 6, 1989. Accepted February 5, 1990.

Multielement Trace Metal Determination by Electrodeposition, Scanning Electron Microscopic X-ray Fluorescence, and Inductively Coupled Plasma Mass Spectrometry

Ngee-Sing Chong, Michael L. Norton,* and James L. Anderson*

Department of Chemistry, University of Georgia, Athens, Georgia 30602

Multielement analysis of multicomponent metallic electrodeposits is described, based on scanning electron microscopy with energy dispersive X-ray fluorescence [EDXRF] detection, followed by dissolution and inductively coupled plasma mass spectrometry [ICP-MS] detection. Application of the method is described for determination of trace elements in seawater, including Zn, Mn, Co, Cu, Cr, Ni, Fe, Cd, Pb, and Hg. These elements are simultaneously electrodeposited onto a niobium wire working electrode at −1.40 V vs an Ag/AgCl reference and subjected to EDXRF analysis. Internal standardization is practical for quantitative calibration at the 1 ppm analyte concentration level in an analyte:internal standard concentration ratio range of 0.02–50. Detection limits for EDXRF range from 1.9 ppb for Fe to 50 ppb for Cd. The deposit is dissolved for subsequent ICP-MS determination. Significant reduction in ICP-MS matrix interferences by Na, Ca, Mg, K, and Cl ions is achieved by deposition at potentials more positive than their very negative reduction potentials. Measurement of elemental isotope ratios is achieved with 0–8% relative error. ICP-MS detection limits for all elements except Zn and Fe are superior to those of EDXRF. Mn, Ni, Cd, Pb, and Hg can easily be determined in the range of 13–86 parts per trillion with ICP-MS.

INTRODUCTION

Determination of trace metals in seawater represents one of the most challenging tasks in chemical analysis because the parts-per-billion (ppb) or sub-ppb levels of analyte are very susceptible to matrix interference from the alkali or alkaline-earth metals and their associated counterions. For instance, the alkali metals tend to affect the atomization and the ionization equilibrium processes in atomic spectroscopy, and the associated counterions such as the chloride ions might be preferentially adsorbed onto the electrode surface to give some undesirable electrochemical side reactions in voltammetric analysis. Thus, most current methods for seawater analysis employ some kind of analyte preconcentratioin along with matrix rejection techniques. These preconcentration techniques include coprecipitation (*1*, *2*), solvent extraction (*3–5*), column adsorption (*4–6*), electrodeposition (*7–10*), and Donnan dialysis (*11*, *12*).

Measurement techniques that can be employed for the determination of trace metals include atomic absorption spectrometry [AAS] (*5*, *7*, *8*), anodic stripping voltammetry (*11*, *13*, *14*), differential pulse cathodic stripping voltammetry (*15*, *16*), inductively coupled plasma atomic emission spectrometry [ICP-AES] (*9*, *12*, *17*), and liquid chromatography of the metal chelates with ultraviolet–visible absorption

0003-2700/90/0362-1043$02.50/0